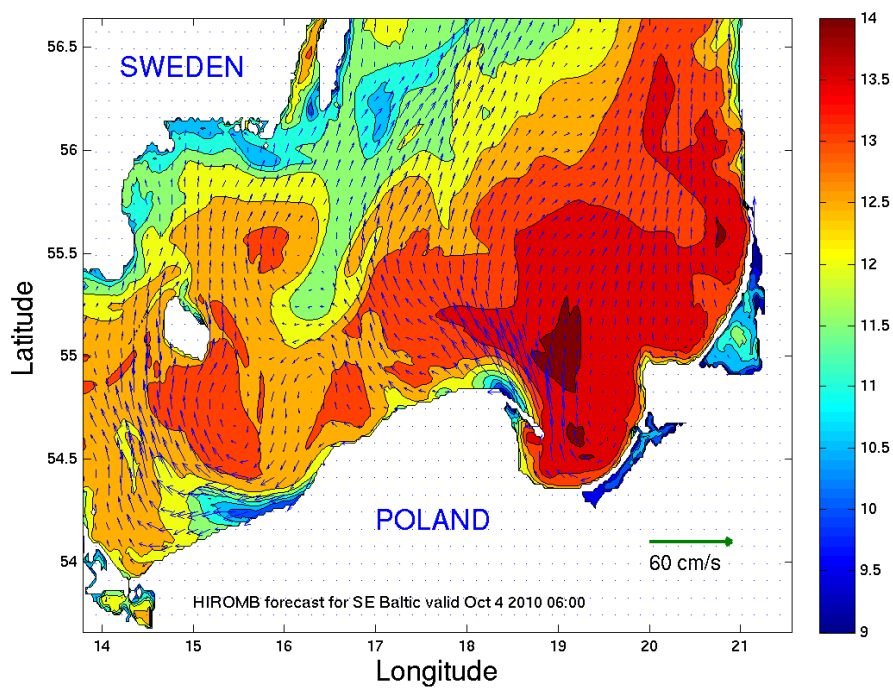


HIROMB

An introduction to HIROMB, an operational baroclinic model for the Baltic Sea

Lennart Funkquist and Eckhard Kleine



Front:

Example of a forecast of sea surface temperature and currents for the SE Baltic
from the operational ocean model HIROMB

ISSN: 0283-1112 © SMHI

REPORT OCEANOGRAPHY No 37, 2007

HIROMB

An introduction to HIROMB, an operational baroclinic model for the Baltic Sea

Lennart Funkquist and Eckhard Kleine

Abstract

A 3-dimensional baroclinic model of the North Sea and the Baltic Sea, designed for a daily operational use is described in detail. The model is based on a similar model running in operational mode at the German Federal Maritime and Hydrographic Agency (BSH) in Hamburg, Germany. The operational forecasts started in 1995 with a daily 24-hour forecast and was later extended to 48 hours. The model is mainly forced by SMHI's operational atmospheric model (HIRLAM), but also by river runoff from an operational hydrological model and wave radiation stress from a wind wave model. The present version of the model is set up on a nested grid where a 12 nautical mile (nm) grid covers the whole area while Skagerrak, Kattegat, the Belt Sea and the Baltic Sea are covered with a 1 nm grid. A parallelized version of the model has been developed and runs on a distributed memory parallel computer.

Contents

1	Introduction	4
2	Grid configuration	5
3	Forcing	6
3.1	Atmospheric forcing	7
3.2	Open boundary forcing	9
3.3	River runoff	11
4	Basic equations	12
4.1	Momentum balance and continuity	12
4.1.1	Hydrostatic approximation	13
4.1.2	Reynolds averaging	13
4.1.3	Boussinesq approximation	15
4.1.4	Vertical integration	15
4.2	Salinity and temperature equations	16
4.3	Horizontal mixing	16
4.4	Vertical mixing	17
4.4.1	Non-local turbulence	19
4.5	Wind wave forcing	20
4.6	Dynamics of sea ice	22
4.7	Thermodynamics of sea ice	25
5	Numerical solution technique	28
5.1	Space discretization	28
5.2	Time discretization	28
6	Parallelization	30
6.1	Modification of the code	31
6.2	Decomposition into blocks	31
6.2.1	Decomposition of ice coverage	32
6.2.2	Data handling	35
6.2.3	Parallel performance	35

1 Introduction

The use of numerical circulation models has a long tradition at SMHI. From the mid 70's, baroclinic 3D models have been used preferably in connection with environmental-oriented problems like spreading of oil, cooling water outlets from power plants and long-term spreading of radio-active substances, see [Simons et al. 1977], [Vasseur et al. 1980], [Funkquist and Gidhagen 1984] and [Funkquist 1985]. Since the 70's there have also been a number of more process-oriented studies for the Baltic Sea with 3D models, e.g. [Simons 1978], [Kielmann 1981], [Lehmann 1995] and [Elken 1996].

However, it was not until 1991 that the first use of an operational circulation model started at SMHI with a vertical integrated model covering the Baltic Sea with a resolution of 5 km and forced by daily weather forecasts and in- and outflow through the Danish Straits [Funkquist 1993]. Later, in 1994 a three-dimensional barotropic version of the POM model (Princeton Ocean Model [Blumberg and Mellor 1987]), covering both the North Sea and the Baltic Sea with 6 vertical levels and a horizontal resolution of 10 km, was set in operational use. With this model it was then possible to give a more accurate forecast of surface currents in all the Swedish coastal water.

At the same time, a fruitful cooperation with the German Federal Maritime and Hydrographic Agency (BSH) started with the aim of a common operational system for the North Sea and Baltic Sea region. BSH already since 1993 had a fully operational model working for the North Sea/Baltic Sea region including an ice module and an interface to a operational wave model [Kleine 1994]. In transferring the BSH model to a more general Baltic Sea model, the main modifications of the model itself only composed of changing the time integration scheme and the nesting from a configuration adapted to the German waters to a more general one.

In connection with the cooperation that started with BSH, a further cooperation with the aim of including all Baltic Sea nations was planned. It was called the HIROMB project and it was stated that the main objectives of the HIROMB co-operation should be:

- i) *The model should constitute the basis for a common operational system for all states surrounding the Baltic Sea.*
- ii) *All states with a border to the Baltic Sea should be invited to the HIROMB project, and the member institute of each state should be appointed by the relevant ministry.*
- iii) *The model should be run at one place where access to a supercomputer could be granted.*
- iv) *The output from the operational run should be distributed to all members of the project.*

v) *Each participating state should contribute equally to the maintenance and development of the system.*

The project got the acronym HIROMB, which stands for High Resolution Operational Model for the Baltic Sea. At the first stage, Germany (BSH) and Sweden (SMHI) were the only members and in 1999 three more countries (Denmark, Finland and Poland) joined the project.

The first pre-operational runs started in summer 1995. At that time, the model was run once daily on a vector-computer (Convex 3840) producing a 24-hour forecast. In 1997, the model was transferred to a CRAY C90 parallel shared memory vector computer at the National Supercomputer Centre in Sweden. This made it possible to increase the forecast length to 48 hours, but still with only one simulation a day. During 1997-99, the model code has successively been parallelized [Wilhelmsson and Schüle 1998] and a special method of partitioning the computational domain has been developed [Rantakokko 1997]. At present (1999), the 1 nm model runs on a distributed memory parallel CRAY T3E computer in parallel with a backup version on a SGI3800 computer.

The model output is archived and all members of the HIROMB project have access to the complete data base via a ftp-server. A WEB-site has been set up for real-time presentation of forecasts together with validation.

What is described in this report regarding model description and its configuration applies to what was run 2003. However, since then a number of improvements and modifications has been done for the whole system and new members have entered the cooperation.

2 Grid configuration

Basically, there are two factors that determine the model area. Firstly, each project member has their own interest area and though the main region of interest is the Baltic Sea, countries like Sweden, Denmark and Germany also have interest in the Kattegat, Skagerrak and the North Sea. Secondly, the model area has an open boundary to the Atlantic and there is no ultimate choice of its location. Both physical and computational aspects have to be taken into consideration, and this has led to the following configuration (see also figure 1 and table 1).

1. **A storm surge model for the NE Atlantic.** This model only supplies that part of the water level at the boundary between the Atlantic and the North Sea that is driven by solely the meteorological forcing. The tidal motion is added as an open boundary condition, treated in a similar manner as salinity and temperature (see section 3.2).

grid	No of points in W-E	No of points in S-N	increment in longitude	increment in latitude
NE Atlantic	52	46	40'	24'
HIROMB 12 nm	105	88	20'	12'
HIROMB 3 nm	294	253	5'	3'
HIROMB 1 nm	752	735	1'40"	1'

Table 1: Horizontal configuration of the HIROMB grids

2. **A nested set of HIROMB modules with a resolution ranging from a relatively coarse level for the North Sea down to 1 nautical mile for the Skagerrak, Kattegat and the Baltic Sea.** The 1 nm grid (see figure 2) covers the entire Baltic Sea. Boundary values at the open western border at 10° E are provided by a coarser 3 nm grid. This grid (see figure 3) covers the waters east of 6° E.

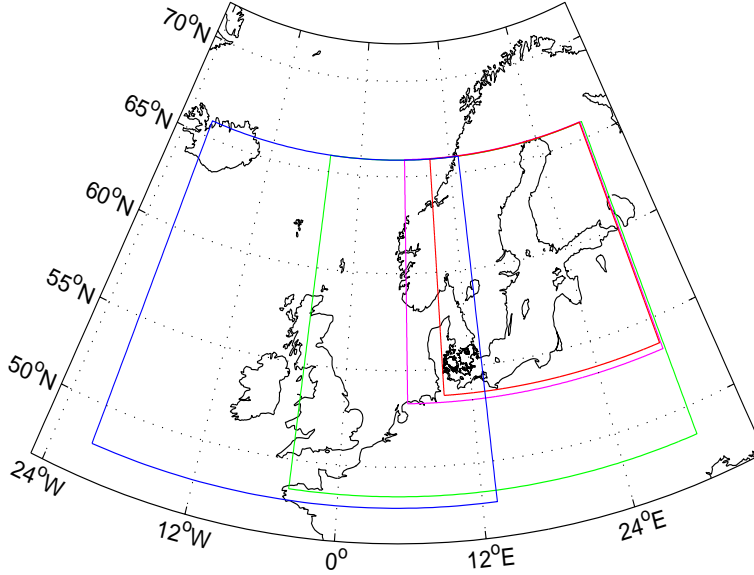


Figure 1: The 12, 3 and 1 nm grids for the 3D model encapsulated by the 24 nm grid for the North-East Atlantic storm surge model.

3 Forcing

HIROMB requires input from both an atmospheric and a hydrological model as well as from an ocean wave model. This dependence on results from other models,

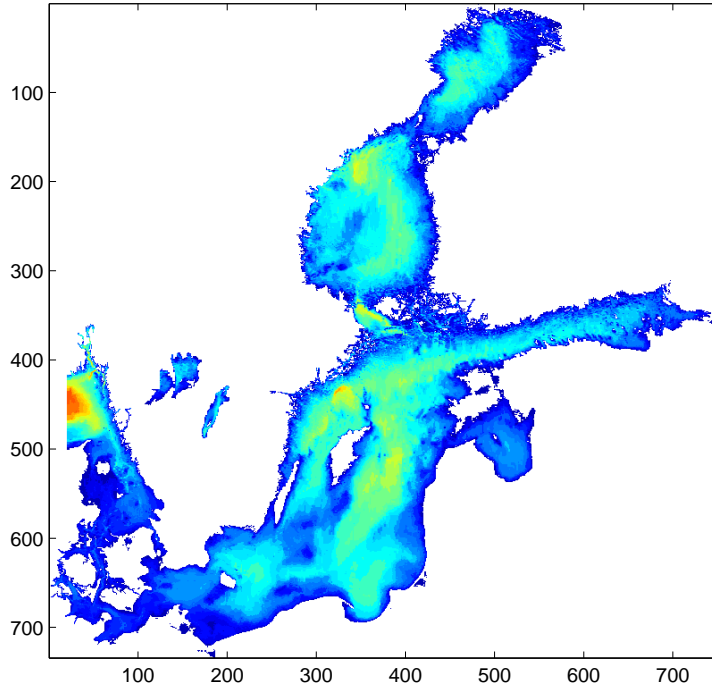


Figure 2: The grid with 1 nm resolution covers the area from Skagerrak to the Baltic Sea. There are 1 126 607 active grid points of which 144 449 are surface points. The maximum depth is 710 *m* in Skagerrak and 460 *m* in the Baltic Sea.

makes HIROMB sensitive to the security of the whole forecast production environment at SMHI. It also has consequences on the delivery time of the HIROMB forecast. However, having all three disciplines at the same institute facilitates a full control of the whole forecast system. In a future perspective, there are plans that the ocean and atmospheric models both will run in parallel, i.e. in a two-way coupled mode.

From 1999, the hydrological model runs in an operational mode. This means that river runoff is available in real-time. The different forcing components are described in detail in the following subsections.

3.1 Atmospheric forcing

The atmospheric model [HIRLAM 1993] provides HIROMB with sea level pressure, wind at 10 m above surface, air temperature and specific humidity at 2 m above surface and total cloudiness. These parameters fully control the momentum and the thermodynamic balance between the sea surface and the atmosphere.

The momentum exchange is computed with a drag formula where the drag

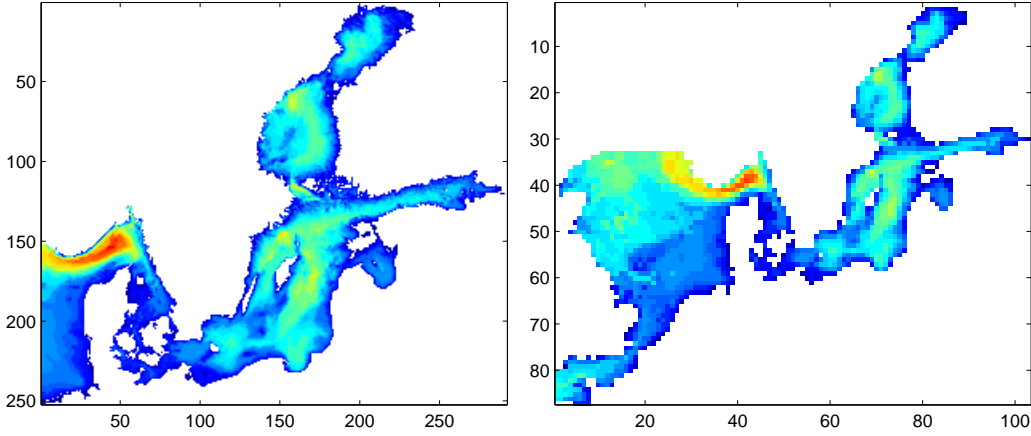


Figure 3: The 3 *nm* grid, to the left has 154 894 active grid points of which 19 073 are surface points. The 12 *nm* grid, to the right, also covers the North Sea and has 9240 active grid points of which 2 171 are surface points.

coefficient is computed by a linear relation to the wind speed at 10*m* height.

$$c_D = 0.001 * (0.7 + 0.09 * \sqrt{u^2 + v^2}) \quad (1)$$

where u and v is the wind velocity components in *m/s*. Ignoring sea ice, the radiation balance can be written as

$$Q = Q_I + Q_B + Q_H + Q_E \quad (2)$$

where Q_I , Q_B , Q_H and Q_E stand for short-wave solar radiation, long-wave radiation, sensible heat flux and latent heat flux respectively. It has been shown [Omstedt and Rutgersson 1998] that the Baltic Sea is almost in thermodynamic equilibrium with the atmosphere averaged over a year. The main contribution comes from the incoming short-wave radiation which as an annual mean is in balance with the heat loss terms.

According to [Shine 1984] we use the following formula for the short-wave insolation.

$$Q_i = Q_0 \frac{s^2}{1.2s + (1 + s) \frac{e_a}{\text{bar}} + 0.046} (1 - 0.6c) \quad (3)$$

where Q_0 is the solar constant, s the sine of inclination of the sun above the horizon according to

$$s = \max(\sin \phi \sin \delta + \cos \phi \cos \delta \cos \omega, 0) \quad (4)$$

where ϕ is the geographical latitude, δ declination angle of the sun and ω the time angle of the local meridian. Q_I is then calculated as $Q_I = (1 - \alpha)Q_i$, where α is the albedo of the water surface and is here set to 0.07 according to [Payne 1972].

The net long-wave radiation is computed with a formula from [Idso and Jackson 1969].

$$Q_B = \varepsilon \sigma (T_a^4 (1 - 0.26 \exp(-7.7 \star 10^{-4} (\frac{T_a}{1K} - 273)^2) (1 - 0.75c^2)) - T_s^4) \quad (5)$$

where ε is the emissivity of the water surface, σ the Stefan-Boltzmann constant, T_s water temperature, T_a air temperature, e_a the water vapour pressure in the atmosphere and c is the cloud coverage ranging from 0 to 1.

The sensible heat flux is driven by the temperature difference between water and air and is expressed as (see [Liu et al. 1979])

$$Q_H = c_{pa} \rho_a c_H (T_a - T_s) W_{10} \quad (6)$$

where c_{pa} is the specific heat of air, ρ air density, c_H diffusivity constant, T_a air temperature, T_s water temperature and W_{10} wind velocity at 10 m height.

In an analogous way, the latent heat flux may be written

$$Q_E = L \rho_a c_E (q_a - q_s) W_{10} \quad (7)$$

where L is the latent heat of evaporation, ρ_a air density, c_e diffusivity constant, q_s specific humidity at sea surface, q_a specific humidity at 10 m height and W_{10} the wind velocity at 10m height.

Please note that the thermodynamic forcing terms are dependent on the SST. Therefore, the atmospheric heat flux cannot be computed in advance, but is determined while HIROMB works. Those basic atmospheric parameters which one-way drive the thermodynamics of HIROMB are air temperature, humidity and cloud cover.

3.2 Open boundary forcing

HIROMB, more precisely the second model in the hierarchy, has an open boundary to the North Atlantic. One part of this boundary line runs through the British Channel, the other makes a straight line between northern Scotland and south-west Norway. Along all that line, water level, salinity and temperature are prescribed at each time step. As described earlier, boundary values of water level come from two sources. They are superposed by the results of a storm surge model for the North Atlantic, which is void of tides, and a setup of 17 tidal constituents, specified for each individual boundary cell.

To supply HIROMB with inflow data of salinity and temperature at its open boundary, we only have climatological fields, month by month. In order to relax their influence on the operational simulation, we have placed a sponge layer along the boundary line. Its purpose is to act as a buffer between the inner model domain

and a "climatological reservoir" outside. We imagine the sponge layer to be a filter literally located in between interior and exterior. It is flushed by the normal flow component as computed next location to the boundary line. That flow either brings a climatological signal or outflow from the interior into the sponge. When flow direction is reversed from outward to inward, it returns what it was filled with, until, in sustained flow, its capacity is exhausted, and it passes more and more of the reservoir. Conversely, for outward flow, the sponge empties into the reservoir which is thought to be of infinite capacity, i.e. does not respond to that input. The performance of the sponge is a matter of its capacity. This capacity should be sufficiently large not to let the reservoir be felt in tidal reversions, but sufficiently small to give an input effect for sustained inflow.

In principle, there are three different types of open boundaries in the model system:

i) *Open boundary between the 2D NE Atlantic storm surge model area and the outer Atlantic*

These boundaries are aligned with latitude and longitude and a radiation condition [Heaps 1974] is used. At the northern, western, southern and eastern boundary respectively, it reads

$$\left. \begin{aligned} c(\zeta - \zeta_0) - Hv &= 0 \\ c(\zeta - \zeta_0) + Hu &= 0 \\ c(\zeta - \zeta_0) + Hv &= 0 \\ c(\zeta - \zeta_0) - Hu &= 0 \end{aligned} \right\} \quad (8)$$

where H is the local depth, $c = \sqrt{gH}$ the local phase velocity and ζ_0 the water elevation caused by the inverse barometric effect, i.e. equal to $\frac{\bar{P}-P}{\rho g}$. Here, P is the local current air pressure, \bar{P} the undisturbed (mean) air pressure and ρ the water density.

ii) *Open boundary conditions for water level between the 3D North Sea/Baltic Sea model and the 2D NE Atlantic storm surge model*

The internally generated tides of the North Sea and the Baltic Sea are negligible because their volume is too small. As an example for the Baltic Sea, the internal tide-generated elevation is only a few centimeters. Thus, all tidal forcing is supplied at the open boundaries between the North Sea and the Atlantic. A large set of observational data available for this open boundary makes it feasible to specify the surface elevation caused by 17 tidal constituents. The total elevation at the boundary is the sum of the surface elevation from the tide and the storm surge generated elevations.

iii) *Open boundary between the different nested grids in the 3D North Sea/Baltic*

Sea model

The coupling between the nested 3D grids is both of a one-way and a two-way type. For salinity and temperature, which are solved numerically by using an explicit time-stepping, the coupling is of a two-way type. On the other hand, when using implicit methods, a two-way coupling is more difficult and for this reason the coupling for variables solved implicitly, i.e. water level and barotropic flow is only one-way.

3.3 River runoff

A river runoff model [Graham 2000] covering the entire Baltic drainage basin, Skagerrak and Kattegat runs on an operational basis at SMHI. The hydrological model produces as output, daily river runoff for 43 sub-basins of which 8 represents the Skagerrak-Kattegat area see figure 4. A further division of the runoff for each sub-basin is made between the major rivers ending up at a total of 82 rivers. Climatological monthly means of river runoff are used as backup if the hydrological model has been out of operation for a week period or longer. Table 3 gives the annual means for 73 rivers.

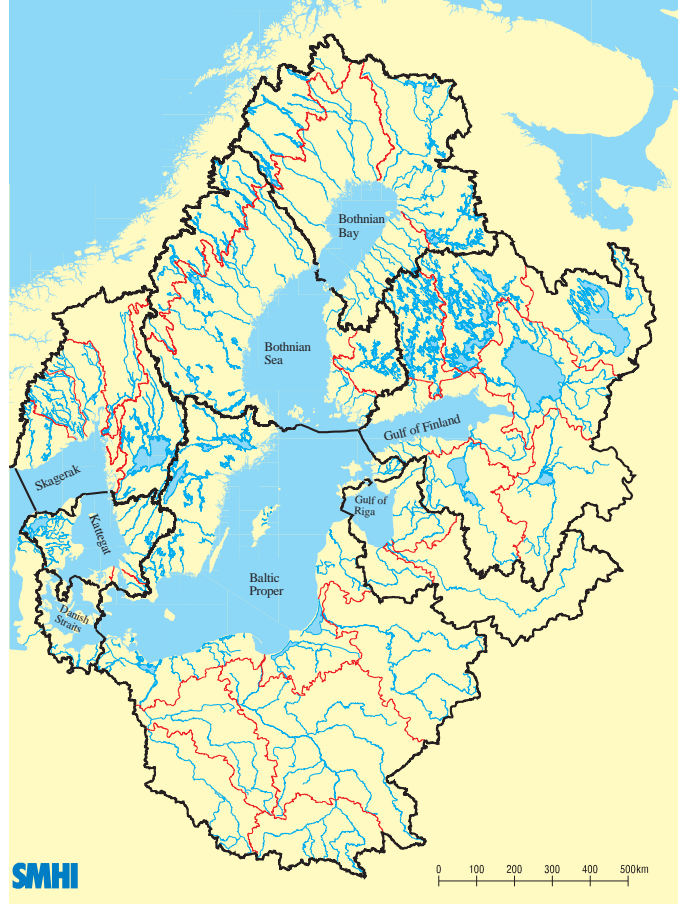


Figure 4: Catchment area for the Baltic Sea, Skagerrak and Kattegat and the distribution of separate drainage basins (red lines) for which the river runoff forecast model is run. Also shown with thick black lines are the sub-basins for a chemical model. Major rivers are marked with blue lines.

4 Basic equations

4.1 Momentum balance and continuity

While the earth is best approximated by an ellipsoid, with the polar and equatorial radius equal to about 6357 km and 6378 km resp., it is most common to use a spherical coordinate system. For the radius of the earth, we use a value (6371 km) of the polar radius which best represents a sphere with equal mass as the earth. The surfaces with equal radius are then thought of as geopotential surfaces, perpendicular to the gravity vector.

The momentum equations expressed in spherical coordinates are easily found in standard text books (see e.g [Gill 1982]). If we neglect the molecular mixing, the equations may be expressed as

$$\left. \begin{aligned} \frac{Du}{Dt} - \frac{\tan \phi}{r} uv + \frac{1}{r} uw &= 2\omega \sin \phi v - 2\omega \cos \phi w - \frac{1}{\rho} \frac{1}{r \cos \phi} \frac{\partial p}{\partial \lambda} \\ \frac{Dv}{Dt} + \frac{\tan \phi}{r} uv + \frac{1}{r} vw &= -2\omega \sin \phi u - \frac{1}{\rho} \frac{1}{r} \frac{\partial p}{\partial \phi} \\ \frac{Dw}{Dt} - \frac{1}{r} uu - \frac{1}{r} vv &= 2\omega \cos \phi u - g - \frac{1}{\rho} \frac{\partial p}{\partial r} \end{aligned} \right\} \quad (9)$$

where ϕ is the latitude, λ the longitude and the r the radius. u , v and w are the velocity components, g acceleration due to gravity ($9.81 m s^{-2}$) and ω the rotation rate of the earth ($7.292 \times 10^{-5} s^{-1}$). The mass conservation equation may be written as

$$\frac{1}{\rho} \frac{D\rho}{Dt} + \frac{1}{r} \frac{\partial u}{\partial \lambda} + \frac{1}{r \cos \phi} \frac{\partial v \cos \phi}{\partial \phi} + \frac{\partial w}{\partial r} = 0 \quad (10)$$

Here $\frac{D}{Dt}$, the total derivative, is given by

$$\frac{D}{Dt} = \frac{\partial}{\partial t} + \frac{u}{r \cos \phi} \frac{\partial}{\partial \lambda} + \frac{v}{r} \frac{\partial}{\partial \phi} + w \frac{\partial}{\partial r} \quad (11)$$

4.1.1 Hydrostatic approximation

A careful examination of the orders of magnitude of the terms in (9) shows that to a high degree of approximation, the vertical momentum balance may be approximated by

$$0 = g + \frac{1}{\rho} \frac{\partial p}{\partial r} \quad (12)$$

This is usually referred to as the hydrostatic approximation.

4.1.2 Reynolds averaging

The flow in the ocean is more or less turbulent and cannot be calculated exactly due to resolution problems connected to limitations in computer capacity. The time scale of the motion that are of interest for an ocean model are far beyond that of the turbulent velocity fluctuations. However, to include the turbulence in the conservations equations above, it is convenient to regard them as applied to a type of mean flow and to treat the fluctuating component in the same manner as the viscous shear stress. Following the statistical approach by Reynolds [Reynolds 1895], we separate the instantaneous values of the velocity components and pressure into a mean and a fluctuating quantity

$$u = \bar{u} + u', \quad v = \bar{v} + v', \quad w = \bar{w} + w', \quad p = \bar{p} + p'$$

where the mean of the fluctuating components is zero by definition and the mean

denoted by a bar is defined as $\bar{u} = \frac{1}{T} \int_0^T u dt$. The averaging period has to be greater than the fluctuating time scale but is more or less artificial as there is hardly no such separation of scales to be found in nature. Averaging the momentum equations and ignoring density fluctuations in the acceleration terms result in a set of equations usually referred to as the Reynolds equations for the mean flow containing terms like: $\overline{\rho u' u'}$, $\overline{\rho u' v'}$, $\overline{\rho u' w'}$ etc.

If we define the vertical coordinate z as $z = r - R$, where R is the radius of our idealized earth, we get with the Reynolds stresses included and neglecting the bar for mean quantities, the following equations.

Momentum balance

$$\left. \begin{aligned} \frac{Du}{Dt} - \frac{\tan \phi}{R} uv + \frac{1}{R} uw + \\ \frac{1}{R \cos \phi} \left(\frac{\partial}{\partial \lambda} (\overline{u' u'}) + \frac{\partial}{\partial \phi} (\cos \phi \overline{u' v'}) + \frac{\partial}{\partial z} (R \cos \phi \overline{u' w'}) \right) - \\ \frac{\tan \phi}{R} \overline{u' v'} + \frac{1}{R} \overline{u' w'} = f v - \frac{1}{\rho} \frac{1}{R \cos \phi} \frac{\partial p}{\partial \lambda} \\ \frac{Dv}{Dt} + \frac{\tan \phi}{R} uv + \frac{1}{R} vw + \\ \frac{1}{R \cos \phi} \left(\frac{\partial}{\partial \lambda} (\overline{v' u'}) + \frac{\partial}{\partial \phi} (\cos \phi \overline{v' v'}) + \frac{\partial}{\partial z} (R \cos \phi \overline{v' w'}) \right) + \\ \frac{\tan \phi}{R} \overline{u' u'} + \frac{1}{R} \overline{v' w'} = -f u - \frac{1}{\rho R} \frac{\partial p}{\partial \phi} \\ 0 = g + \frac{1}{\rho} \frac{\partial p}{\partial z} \end{aligned} \right\} \quad (13)$$

The new terms are called the Reynolds stresses and represent the non-resolved scales of motion, i.e. what we here regard as turbulence. However, as the new set of equations is not closed, we have to express the Reynolds stress terms in the mean quantities. The normal approach to this closure problem is to make use of the analogy with molecular viscosity concepts as was first outlined by Stokes [Stokes 1845] and Boussinesq [Boussinesq 1877]. This means that the stress components are expressed as proportional to an eddy viscosity times the strain-rate of the mean flow. In a spherical coordinate system, we get for the stress terms the following expressions

$$\left. \begin{aligned} -\overline{u' u'} &= 2K \left(\frac{1}{R \cos \phi} \frac{\partial \bar{u}}{\partial \lambda} - \frac{\tan \phi}{R} \bar{v} \right) - \frac{2K}{3} \text{div}(\bar{u}, \bar{v}, \bar{w}) - \frac{2k}{3} \\ -\overline{v' u'} &= K \left(\frac{1}{R} \frac{\partial \bar{u}}{\partial \phi} + \frac{\tan \phi}{R} \bar{u} + \frac{1}{R \cos \phi} \frac{\partial \bar{v}}{\partial \lambda} \right) \\ -\overline{w' u'} &= K \left(\frac{\partial \bar{u}}{\partial z} + \frac{1}{R \cos \phi} \frac{\partial \bar{w}}{\partial \lambda} \right) \\ -\overline{u' v'} &= K \left(\frac{1}{R \cos \phi} \frac{\partial \bar{v}}{\partial \lambda} + \frac{1}{R} \frac{\partial \bar{u}}{\partial \phi} + \frac{\tan \phi}{R} \bar{u} \right) \\ -\overline{v' v'} &= 2K \left(\frac{1}{R} \frac{\partial \bar{v}}{\partial \phi} \right) - \frac{2K}{3} \text{div}(\bar{u}, \bar{v}, \bar{w}) - \frac{2k}{3} \\ -\overline{w' v'} &= K \left(\frac{\partial \bar{v}}{\partial z} + \frac{1}{R} \frac{\partial \bar{w}}{\partial \phi} \right) \\ -\overline{u' w'} &= K \left(\frac{1}{R \cos \phi} \frac{\partial \bar{w}}{\partial \lambda} + \frac{\partial \bar{u}}{\partial z} \right) \\ -\overline{v' w'} &= K \left(\frac{1}{R} \frac{\partial \bar{w}}{\partial \phi} + \frac{\partial \bar{v}}{\partial z} \right) \\ -\overline{w' w'} &= 2K \frac{\partial \bar{w}}{\partial z} - \frac{2K}{3} \text{div}(\bar{u}, \bar{v}, \bar{w}) - \frac{2k}{3} \end{aligned} \right\} \quad (14)$$

where K is an eddy viscosity and k denotes the fluctuating part of the kinetic energy, i.e. $\frac{1}{2}(\overline{u' u'} + \overline{v' v'} + \overline{w' w'})$. We also have defined the vertical coordinate z

as $z = r - R$, where R is the radius of our idealized earth, and approximated r by R when it appears only as a coefficient.

4.1.3 Boussinesq approximation

A further approximation is the quasi-Boussinesq approximation [Boussinesq 1877], which means that the continuity equation is replaced by the incompressibility condition and that density variations are neglected in the inertia term but retained in the buoyancy-force term only. This is justified because variations in density are normally much smaller than the mean density, i.e. $\frac{\rho'}{\rho} \ll 1$. From the incompressibility assumption it follows that the divergence of the flow is zero, i.e.

$$\text{div}(u, v, w) = \frac{1}{r \cos \phi} \left(\frac{\partial u}{\partial \lambda} + \frac{\partial(\cos \phi v)}{\partial \phi} \right) + \frac{\partial w}{\partial z} = 0 \quad (15)$$

Equation of continuity

$$\frac{1}{R \cos \phi} \left(\frac{\partial u}{\partial \lambda} + \frac{\partial(\cos \phi v)}{\partial \phi} \right) + \frac{\partial w}{\partial z} = 0 \quad (16)$$

4.1.4 Vertical integration

By integrating the continuity equation(16) from the bottom, $z = -H(\lambda, \phi)$, to the surface, $z = \zeta(\lambda, \phi, t)$, we are able to construct an equation for the water (surface) level. The integration gives

$$\int_{-H}^{\zeta} \left(\frac{1}{R \cos \phi} \left(\frac{\partial u}{\partial \lambda} + \frac{\partial(\cos \phi v)}{\partial \phi} \right) + \frac{\partial w}{\partial z} \right) dz = 0 \quad (17)$$

The kinematic boundary conditions at bottom and surface are

$$\left. \begin{aligned} \frac{D}{Dt}(z + H(\lambda, \phi)) &= 0 \\ \frac{D}{Dt}(z - \zeta(\lambda, \phi, t)) &= 0 \end{aligned} \right\} \quad (18)$$

or

$$\left. \begin{aligned} w|_B + \frac{1}{R \cos \phi} H_\lambda u|_B + \frac{1}{R} v|_B &= 0 \\ w|_S - \frac{1}{R \cos \phi} \zeta_\lambda u|_S - \frac{1}{R} v|_S - \zeta_t &= 0 \end{aligned} \right\} \quad (19)$$

Replacing for w in the integrated continuity equation gives

$$\begin{aligned} \int_{-H}^{\zeta} \frac{1}{R \cos \phi} \left(\frac{\partial u}{\partial \lambda} + \frac{\partial(\cos \phi v)}{\partial \phi} \right) dz + \frac{1}{R \cos \phi} \zeta_\lambda u|_S + \frac{1}{R} \zeta_\phi v|_S + \\ \zeta_t + \frac{1}{R \cos \phi} H_\lambda u|_B + \frac{1}{R} H_\phi v|_B = 0 \end{aligned} \quad (20)$$

or

$$\frac{1}{R \cos \phi} \frac{\partial}{\partial \lambda} \left(\int_{-H}^{\zeta} u dz \right) + \frac{1}{R \cos \phi} \frac{\partial}{\partial \phi} \left(\int_{-H}^{\zeta} \cos \phi v dz \right) + \zeta_t = 0 \quad (21)$$

If $p_a(\lambda, \phi)$ denotes the atmospheric pressure at sea surface, the hydrostatic equation (12) can be integrated to give the following expression for the pressure in the horizontal momentum equations

$$p(\lambda, \phi, z) = p_a(\lambda, \phi) + \int_z^{\zeta(\lambda, \phi)} g \rho(\lambda, \phi, z) dz \quad (22)$$

4.2 Salinity and temperature equations

Again ignoring molecular viscosity and applying the continuity equation and the Boussinesq approximation, we get the following equations for salinity and temperature

$$\left. \begin{aligned} \frac{\partial S}{\partial t} + \text{div}(uS, vS, wS) &= 0 \\ \frac{\partial T}{\partial t} + \text{div}(uT, vT, wT) &= 0 \end{aligned} \right\} \quad (23)$$

By applying the same method of Reynolds averaging as for the momentum equations, we have

$$\left. \begin{aligned} \frac{DS}{Dt} &= \frac{1}{R \cos \phi} \left(\frac{\partial(-\overline{u'S'})}{\partial \lambda} + \frac{\partial(-\cos \phi \overline{v'S'})}{\partial \phi} \right) + \frac{\partial(-\overline{w'S'})}{\partial z} \\ \frac{DT}{Dt} &= \frac{1}{R \cos \phi} \left(\frac{\partial(-\overline{u'T'})}{\partial \lambda} + \frac{\partial(-\cos \phi \overline{v'T'})}{\partial \phi} \right) + \frac{\partial(-\overline{w'T'})}{\partial z} \end{aligned} \right\} \quad (24)$$

The expressions for the Reynolds stress terms analogous to the momentum equations are

$$\left. \begin{aligned} -\overline{u'S'} &= M_h \frac{1}{R \cos \phi} \frac{\partial \overline{S}}{\partial \lambda} \\ -\overline{v'S'} &= M_h \frac{1}{R} \frac{\partial \overline{S}}{\partial \phi} \\ -\overline{w'S'} &= M_v \frac{\partial \overline{S}}{\partial z} \\ -\overline{u'T'} &= M_h \frac{1}{R \cos \phi} \frac{\partial \overline{T}}{\partial \lambda} \\ -\overline{v'T'} &= M_h \frac{1}{R} \frac{\partial \overline{T}}{\partial \phi} \\ -\overline{w'T'} &= M_v \frac{\partial \overline{T}}{\partial z} \end{aligned} \right\} \quad (25)$$

Temperature and salinity are coupled to the momentum equations by the equation of state

$$\varrho = \varrho(S, T, p) \quad (26)$$

In the HIROMB model ϱ is computed with the UNESCO formula ([Gill 1982]).

4.3 Horizontal mixing

Depending on the large difference in scales between the horizontal and vertical motion in the ocean, the eddy viscosity for horizontal motion is several orders of magnitude greater than the vertical one. In the horizontal, we use the approach

by Smagorinsky [Smagorinsky 1963]. Denoting the horizontal eddy viscosity by K_h , the horizontal stresses can be expressed as

$$\left. \begin{aligned} -\overline{u'u'} &= K_h D_t - k \\ -\overline{u'v'} &= K_h D_s \\ -\overline{v'v'} &= -K_h D_t - k \end{aligned} \right\} \quad (27)$$

where D_t denotes the horizontal stretching rate defined as

$$D_t = \frac{1}{R \cos \phi} \frac{\partial u}{\partial \lambda} - \frac{1}{R} \frac{\partial v}{\partial \phi} - \frac{\tan \phi}{R} v \quad (28)$$

D_s denotes the horizontal shearing deformation defined as

$$D_s = \frac{1}{R} \frac{\partial u}{\partial \phi} + \frac{\tan \phi}{R} u + \frac{1}{R \cos \phi} \frac{\partial v}{\partial \lambda} \quad (29)$$

and

$$k = (\overline{u'u'} + \overline{v'v'})/2 \quad (30)$$

The horizontal eddy viscosity may then be expressed as

$$K_h = L_h^2 D \quad (31)$$

where L_h is a horizontal length scale and D denotes an invariant of the deformation rate tensor.

$$D = \sqrt{D_s^2 + D_t^2} \quad (32)$$

For the length scale we use the formula by Smagorinsky [Smagorinsky 1963]

$$L_h^2 = (\kappa R \cos \phi \Delta \lambda) * (\kappa R \Delta \phi) \quad (33)$$

where $\kappa = 0.4$. For the eddy diffusivity we simply use the formula $M_h = K_h$

4.4 Vertical mixing

The shear stress terms (vertical flux of horizontal momentum) are

$$-\overline{w'u'} = K_v \frac{\partial u}{\partial z} \quad (34)$$

$$-\overline{w'v'} = K_v \frac{\partial v}{\partial z} \quad (35)$$

and in analogy with the horizontal mixing, we define the vertical eddy viscosity as

$$K_v = L_v^2 \psi \quad (36)$$

where L_v is a vertical length scale and ψ is defined as

$$\psi = \sqrt{\bar{u}_z^2 + \bar{v}_z^2} \quad (37)$$

In its present version, HIROMB makes use of a diagnostic formula for eddy viscosity. It is of type (36), i.e. based on diagnosed length scale and time scale. To arrive at a formula for the vertical turbulent length scale, we first introduce the following parameters

The flux Richardson number:

$$Ri_f = -\frac{g\overline{\rho'w'}}{\rho(\overline{u'w'u_z} + \overline{v'w'v_z})} \quad (38)$$

The gradient Richardson number:

$$Ri_g = -\frac{g\rho_z}{\rho(u_z^2 + v_z^2)} \quad (39)$$

where z is defined in $[-H \leq z \leq \zeta]$

The turbulent Prandtl number:

$$Pr = \frac{Ri_g}{Ri_f} = \frac{K_v}{M_v} \quad (40)$$

The turbulence model by [Mellor and Yamada 1974] gives a functional dependence between Pr and Ri_g

$$Pr = \frac{Ri_g}{0.725(Ri_g + 0.186 - \sqrt{Ri_g^2 - 0.316 Ri_g + 0.0346})} \quad (41)$$

or

$$\frac{1}{Pr} = \frac{0.725 * 0.688}{(Ri_g + 0.186 + \sqrt{Ri_g^2 - 0.316 Ri_g + 0.0346})} \quad (42)$$

From this it follows that

$$Ri_f = Ri_f(Ri_g) = \frac{1}{Pr} Ri_g \quad (43)$$

For the length scale we use a generalization of the von Karman formula proposed by Laikhtman [Laikhtman 1979] and expressed as

$$L = \kappa \frac{\psi(1 - 4 Ri_f)}{|(\psi(1 - 4 Ri_f))_z|} \quad (44)$$

where $\psi = \sqrt{u_z^2 + v_z^2}$. In case of strong variations in the length scale, a smoothing procedure has been added. Then, the effective length scale L_v comes from the relaxation equation

$$\frac{d L_v}{dt} = \psi(L - L_v) \quad (45)$$

This equation reminds one on a dynamic length scale balance equation. However, no claim is raised, and its intended purpose is nothing but filtering. In this way, we may likewise construct a similar equation for the vertical eddy viscosity

$$\frac{\partial}{\partial t} K_v = \frac{\psi}{4}(L_v \varphi - K_v) \quad (46)$$

4.4.1 Non-local turbulence

For any z along the vertical, i.e. $[-H \leq z \leq \zeta]$, consider the following integral expressions

$$L_v^d(z) = \int_0^{H+z} 2\kappa \exp\left(-\int_{z-\delta}^z \frac{\kappa d\xi}{\mathcal{L}(\xi)}\right) d\delta \quad (47)$$

$$L_v^u(z) = \int_0^{\zeta-z} 2\kappa \exp\left(-\int_z^{z+\delta} \frac{\kappa d\xi}{\mathcal{L}(\xi)}\right) d\delta \quad (48)$$

$$\varphi^d(z) = \int_0^{H+z} \kappa \exp\left(-\int_{z-\delta}^z \frac{\kappa d\xi}{\mathcal{L}(\xi)}\right) \psi(z - \delta) d\delta \quad (49)$$

$$\varphi^u(z) = \int_0^{\zeta-z} \kappa \exp\left(-\int_z^{z+\delta} \frac{\kappa d\xi}{\mathcal{L}(\xi)}\right) \psi(z + \delta) d\delta \quad (50)$$

These terms are based on master distributions of local scales of length \mathcal{L} and frequency ψ . They are constructed to give integral scales of length L_v and velocity φ . The idea behind is Prandtl's picture about the action of turbulence in mixing. A parcel of fluid is considered and followed when it undergoes turbulent excursions. During its travel, it is continuously disintegrated. In the sense of Prandtl, mixing length is the statistical distance which is travelled through in the process of disintegration. Here, we are concerned with vertical length scales, i.e. travel distances along the vertical. We distinguish between upward and downward excursions, hence the superscripts u and d . A contribution to mixing might come from any location on the vertical. Therefore, with respect to any reference location - point of start - an integral is formed over all the vertical, up to surface and down to bottom. At each point we fix a dimensionless weight which returns its contribution to the mixing process. We imagine a probing through the water column. In determining the length scale, this distribution of weights is integrated over the vertical. The integration variable δ is nothing but the travel distance, always positive. The more

weight is placed at far distances, the greater the length scale. Please note that the weight distribution always decreases as the probing distance increases.

Of course, the resulting formula has to be consistent with common findings. In particular, it has to return the well-known Karman length scale formula for a logarithmic shear layer. As is not difficult to check, this condition is met by what we take as the contrived mixing density distribution, see the formula.

Based on this consideration, we go one more step further to also set up an integral formula for velocity scale. Applying the formula to the example of a logarithmic shear layer, it becomes clear how an upward and downward integral have to be combined. We arrive at

$$L_v(z) = \min(L_v^d(z), L_v^u(z)) \quad (51)$$

$$\varphi(z) = \max(\varphi^d(z), \varphi^u(z)) \quad (52)$$

In our application, we insert the Karman-Laikhtman scale (44) for \mathcal{L} .

4.5 Wind wave forcing

From the viewpoint of a filtered model (large scale, slow evolution), waves make a subscale process. The presence of waves gives a net effect which comes from self-correlation. The Stokes drift is a mass flow which originates from correlation between surface elevation and flow. In an oscillating wave, forward flow and backward flow do not exactly cancel out but leave a net flow. In the momentum equations, the quadratic terms also leave a non-vanishing effect on averaging. Thus, although waves are a much faster phenomenon than what a filtered model is designed to do, their presence should not be neglected. This is the more necessary the more intense the waves are, because the filter effect is non-linear with respect to wave characteristics.

Unlike entirely irregular turbulent fluctuations, waves are much more accessible to modelling. In our context, we employ a phase-averaged model which describes the comparatively slow evolution of wave energy quantities. There are several such models at various levels. In our case, use is made of the 2nd generation model HYPAS [Günther and Rosenthal 1983], where the shorthand stands for HYbrid PArametric and Shallow. In that model, the entire wave energy spectrum is composed in a hybrid way of wind-sea and swell. Either component is given in a simple form which depends on only a few parameters. A parameterization is also applied to the influence of water depth. HYPAS provides what may be considered as the "wave forcing" for HIROMB. Thus, as for HIRLAM, it is run independently and in advance of HIROMB.

To account for the effect of waves, the following 6 parameters are extracted from the operational wave model

1. wind wave energy
2. peak frequency of wind waves
3. dominant direction of wind waves
4. swell energy
5. peak frequency of swell
6. dominant direction of swell

In a linear approximation the wind waves may be regarded as a superposition of harmonic waves obeying the dispersion relation

$$\omega^2 = gk \tanh(kh) \quad (53)$$

where ω is the frequency, k the wave number and h the water depth. For deep water the dispersion relation reduces to

$$\omega^2 = gk \quad (54)$$

From the above formula, we also get for the phase velocity c and group velocity c_g the following formulae

$$\begin{aligned} c^2 &= \frac{g}{k} \tanh(kh) \\ c_g &= c \frac{1}{2} \left(1 + \frac{2kh}{\sinh(2kh)} \right) \end{aligned} \quad (55)$$

The wave amplitude and orbital velocities may be treated as fluctuations from the mean. With the input of energy, frequency and direction from the wave model, the fluctuations will then take the following form

$$\left. \begin{aligned} \zeta' &= A \cos(\alpha - \omega t) \\ u' &= A\omega \frac{\cosh(k(H+z))}{\sinh(kh)} \cos(\alpha - \omega t) \sin \theta \\ v' &= A\omega \frac{\cosh(k(H+z))}{\sinh(kh)} \cos(\alpha - \omega t) \cos \theta \frac{1}{\cos \theta} \\ w' &= A\omega \frac{\sinh(k(H+z))}{\sinh(kh)} \sin(\alpha - \omega t) \end{aligned} \right\} \quad (56)$$

where A is the amplitude, and θ the direction of a harmonic wave. Because of continuity, the phase angle α has to obey the following formula

$$\sin \theta \frac{\partial \alpha}{\partial \lambda} + \cos \theta \frac{\partial \alpha}{\partial \phi} = kR \cos \phi \quad (57)$$

For the Reynolds stress terms in the momentum equations, we get by substituting

for the fluctuating quantities from equation(56)

$$\left. \begin{aligned} \cos \phi \overline{u'u'} &= \frac{1}{2} A^2 \omega^2 \frac{\cosh^2(k(h+z))}{\sinh^2(kh)} \sin^2 \theta \cos \phi \\ \cos^2 \phi \overline{u'v'} &= \frac{1}{2} A^2 \omega^2 \frac{\cosh^2(k(h+z))}{\sinh^2(kh)} \cos \theta \sin \theta \cos \phi \\ \cos^2 \phi \overline{u'w'} &= 0 \\ \overline{v'u'} &= \frac{1}{2} A^2 \omega^2 \frac{\cosh^2(k(h+z))}{\sinh^2(kh)} \sin \theta \cos \theta \frac{1}{\cos \phi} \\ \cos \phi \overline{v'v'} &= \frac{1}{2} A^2 \omega^2 \frac{\cosh^2(k(h+z))}{\sinh^2(kh)} \cos^2 \theta \frac{1}{\cos \phi} \\ \cos \phi \overline{v'w'} &= 0 \end{aligned} \right\} \quad (58)$$

By vertical integration of the momentum equations, it is also possible to calculate the influence of wind waves on the large-scale volume fluxes. Using (55) we get for the vertical integration of the z-dependent term in (56)

$$\int_{-H}^{\zeta} \frac{\cosh^2(k(H+z))}{\sinh^2(kh)} dz = \frac{1}{k} \frac{c_g}{c} \coth(kh) = \frac{c_g}{c} \frac{g}{\omega^2} \quad (59)$$

where we also have used the equipartition property of wind wave energy, i.e. $E = \frac{1}{2} A^2$ with E denoting the energy. The wave-induced fluxes then become

$$\left. \begin{aligned} \int_{-H}^{\zeta} \cos \phi \overline{u'u'} &= g E \frac{c_g}{c} \sin^2 \theta \cos \phi \\ \int_{-H}^{\zeta} \cos^2 \phi \overline{u'v'} &= g E \frac{c_g}{c} \cos \theta \sin \theta \cos \phi \\ \int_{-H}^{\zeta} \overline{v'u'} &= g E \frac{c_g}{c} \sin \theta \cos \theta \frac{1}{\cos \phi} \\ \int_{-H}^{\zeta} \cos \phi \overline{v'v'} &= g E \frac{c_g}{c} \cos^2 \theta \frac{1}{\cos \phi} \end{aligned} \right\} \quad (60)$$

Similarly we get for the wind wave terms in the continuity equations

$$\left. \begin{aligned} \overline{\zeta'u'}|_{z=\zeta} &= \frac{1}{2} A^2 \omega \coth(kh) \sin \theta = g \frac{E}{c} \sin \theta \\ \overline{\zeta' \cos \phi v'}|_{z=\zeta} &= \frac{1}{2} A^2 \omega \coth(kh) \cos \theta = g \frac{E}{c} \cos \theta \end{aligned} \right\} \quad (61)$$

This net volume flux corresponds to the Stoke's drift.

4.6 Dynamics of sea ice

The ice model consists of two main components: thermodynamics, i.e. growth and melting, and dynamics, i.e. drift. As for any other large-scale sea ice model, the ice drift model is based on continuum mechanics. The ice mechanics model computes forces and deformation. Thus, its components are an equation of motion (momentum budget) and a constitutive equation which gives the response of the ice to deformation. To close the system, there are also evolution equations for the remaining budget quantities.

The basic equations for momentum balance of sea ice come from 2D-continuum mechanics, in the case of plane stress. In spherical coordinates, we have

$$\left. \begin{aligned} \rho_i h \left(\frac{\partial u}{\partial t} + \frac{u}{R \cos \phi} \frac{\partial u}{\partial \lambda} + \frac{v}{R} \frac{\partial u}{\partial \phi} - \left(\frac{\tan \phi}{R} u + f \right) v + g \frac{1}{R \cos \phi} \frac{\partial \zeta}{\partial \lambda} \right) &= \tau_w^\lambda + \tau_a^\lambda + F^\lambda \\ \rho_i h \left(\frac{\partial v}{\partial t} + \frac{u}{R \cos \phi} \frac{\partial v}{\partial \lambda} + \frac{v}{R} \frac{\partial v}{\partial \phi} + \left(\frac{\tan \phi}{R} u + f \right) u + g \frac{1}{R} \frac{\partial \zeta}{\partial \phi} \right) &= \tau_w^\phi + \tau_a^\phi + F^\phi \end{aligned} \right\} \quad (62)$$

where

$$\left. \begin{aligned} \tau_w^\lambda &= c_w \rho_w ((u_w - u)^2 + (v_w - v)^2)^{1/2} (u_w - u) \\ \tau_w^\phi &= c_w \rho_w ((u_w - u)^2 + (v_w - v)^2)^{1/2} (v_w - v) \\ \tau_a^\lambda &= c_a \rho_a ((u_a - u)^2 + (v_a - v)^2)^{1/2} (u_a - u) \\ \tau_a^\phi &= c_a \rho_a ((u_a - u)^2 + (v_a - v)^2)^{1/2} (v_a - v) \end{aligned} \right\} \quad (63)$$

and

$$\left. \begin{aligned} F^\lambda &= \frac{1}{R \cos \phi} \left(\frac{\partial}{\partial \lambda} (\sigma_{11}) + \frac{\partial}{\partial \phi} (\cos \phi \sigma_{12}) \right) - \frac{\tan \phi}{R} \sigma_{12} \\ F^\phi &= \frac{1}{R \cos \phi} \left(\frac{\partial}{\partial \lambda} (\sigma_{21}) + \frac{\partial}{\partial \phi} (\cos \phi \sigma_{22}) \right) + \frac{\tan \phi}{R} \sigma_{11} \end{aligned} \right\} \quad (64)$$

To characterize the deformation properties of the hypothesized large-scale continuum mechanics material, use is made of Reiner-Rivlin equations as the general form of constitutive equations of a fluid. (Note that a fluid has no reference configuration. Thus, elastic phenomena are excluded.)

$$\left. \begin{aligned} \sigma_{11} &= \zeta (\dot{\epsilon}_{11} + \dot{\epsilon}_{22}) + \eta (\dot{\epsilon}_{11} - \dot{\epsilon}_{22}) - \frac{P}{2} \\ \sigma_{12} &= 2\eta \dot{\epsilon}_{12} \\ \sigma_{21} &= 2\eta \dot{\epsilon}_{21} \\ \sigma_{22} &= \zeta (\dot{\epsilon}_{22} + \dot{\epsilon}_{11}) + \eta (\dot{\epsilon}_{22} - \dot{\epsilon}_{11}) - \frac{P}{2} \end{aligned} \right\} \quad (65)$$

In spherical coordinates, the rates of deformation read

$$\left. \begin{aligned} \dot{\epsilon}_{11} &= \frac{1}{R \cos \phi} \frac{\partial u}{\partial \lambda} - \frac{\tan \phi}{R} v \\ \dot{\epsilon}_{12} &= \dot{\epsilon}_{21} = \frac{1}{2} \left(\frac{1}{R} \frac{\partial u}{\partial \phi} + \frac{\tan \phi}{R} u + \frac{1}{R \cos \phi} \frac{\partial v}{\partial \lambda} \right) \\ \dot{\epsilon}_{22} &= \frac{1}{R} \frac{\partial v}{\partial \phi} \end{aligned} \right\} \quad (66)$$

It is assumed that large-scale pack ice is isotropic so that its mechanical behaviour may be stated in terms of invariants of stress and strain rate

$$\left. \begin{aligned} \sigma_I &= \frac{1}{2} (\sigma_{11} + \sigma_{22}) \\ \sigma_{II} &= \frac{1}{2} ((\sigma_{11} - \sigma_{22})^2 + 4\sigma_{12}\sigma_{21})^{1/2} \end{aligned} \right\} \quad (67)$$

$$\left. \begin{aligned} \dot{\epsilon}_I &= (\dot{\epsilon}_{11} + \dot{\epsilon}_{22}) \\ \dot{\epsilon}_{II} &= ((\dot{\epsilon}_{11} - \dot{\epsilon}_{22})^2 + 4\dot{\epsilon}_{12}\dot{\epsilon}_{21})^{1/2} \end{aligned} \right\} \quad (68)$$

Given these definitions, the constitutive equations, in terms of invariants, read

$$\left. \begin{aligned} \sigma_I + \frac{P}{2} &= \zeta \dot{\epsilon}_I \\ \sigma_{II} &= \eta \dot{\epsilon}_{II} \end{aligned} \right\} \quad (69)$$

where $P/2$ is a reference pressure while ζ and η are viscosities. In Hibler's famous viscous-plastic sea ice model [Hibler 1979], these viscosities are specified as follows.

Let

$$\Delta = (\dot{\epsilon}_I^2 + (\dot{\epsilon}_{II}/e)^2)^{1/2} \quad \} \quad (70)$$

be one more invariant of the strain-rate tensor, Δ_0 some low reference value, and put

$$\begin{aligned} \zeta &= \frac{1}{\max(\Delta, \Delta_0)} \frac{P}{2} \\ \eta &= \frac{1}{e^2} \zeta \end{aligned} \quad (71)$$

As is not difficult to see, the state of stress is confined to the yield ellipse

$$(\sigma_I + \frac{P}{2})^2 + (e\sigma_{II})^2 = \frac{\Delta^2}{(\max(\Delta, \Delta_0))^2} (\frac{P}{2})^2 \leq (\frac{P}{2})^2 \quad (72)$$

Here, we recognize the meaning of e . It is the excentricity of the yield ellipse(72).

Here, Hiblers model is stated for the sake of reference. In HIROMB, a modification is implemented, however. As has turned out in a mathematical investigation [Kleine and Sklyar 1995], it is appropriate to relax Hibler's rigid plasticity by admitting that the yield curve is exceeded. For sufficiently large rates of strain, it should be possible to attain any stress. In practice, such should be the case only in a neighbourhood of the yield curve, however.

Thus, the constitutive equation of HIROMB's ice model is viscous-viscoplastic rather than viscous-plastic. We take some very small non-dimensional $\kappa > 0$ parameter and let

$$\begin{aligned} \zeta &= \frac{1 + \kappa \max(\frac{\Delta}{\Delta_0} - 1, 0)}{\max(\Delta, \Delta_0)} \frac{P}{2} \\ \eta &= \frac{1}{e^2} \zeta \end{aligned} \quad \} \quad (73)$$

Compared to (72), we now have

$$((\sigma_I + \frac{P}{2})^2 + (e\sigma_{II})^2)^{1/2} = \frac{\Delta}{\Delta_0} \frac{\Delta_0 + \kappa \max(\Delta - \Delta_0, 0)}{\max(\Delta, \Delta_0)} \frac{P}{2} \quad (74)$$

As shown in [Kleine and Sklyar 1995], introducing the parameter κ as a (minor) modification of Hibler's model amounts to regularizing the ice mechanics problem.

As a closure of the ice dynamics model, there are two budget equations for areal density and compactness. In the compactness equation, a ridging term (sink of compactness) is involved to prevent it from exceeding unity.

$$\frac{\partial h}{\partial t} + \frac{1}{R \cos \phi} \left(\frac{\partial(uh)}{\partial \lambda} + \frac{\partial(\cos \phi v h)}{\partial \phi} \right) = 0 \quad (75)$$

$$\frac{\partial A}{\partial t} + \frac{1}{R \cos \phi} \left(\frac{\partial(uA)}{\partial \lambda} + \frac{\partial(\cos \phi v A)}{\partial \phi} \right) = \mathcal{R} \quad (76)$$

While the total mass of ice, given by its areal density h is conserved under transport, compactness in general is not. To prevent local compactness from exceeding unity, as could happen in cases of convergence, a sink term, the so-called ridging function \mathcal{R} , appears on r.h.s. Keep in mind that there is no fundamental principle on which (76) is based.

4.7 Thermodynamics of sea ice

Growth and melting of sea ice is controlled by the heat budget of the ice cover. In the model, the ice is considered as a plane slab. Its bulk heat budget is given by

$$Q + Q^o = \varrho c_p h \frac{d\bar{T}}{dt} - \varrho L \frac{dh}{dt} \quad (77)$$

where the following notation is used: Q atmospheric heat flux at ice surface, Q^o oceanic heat flux at ice bottom, ϱ ice density, c_p specific heat capacity of ice, h ice thickness, \bar{T} mean ice temperature. Both (external) heat fluxes are taken positive if directed into the ice. On the left-hand side of (77), there is the heat input into the ice while the contributions to r.h.s come from heating/cooling and phase change by growing/melting.

As with surface temperature in modelling atmospheric heat flux over open ocean, the ice temperature is part of the problem, i.e. to be determined. We have to obtain both temperature and thickness from (77).

To tackle the problem, we need more insight. On the vertical, let the ice slab be an interval, say $z_B < z < z_S$ so that $h = z_S - z_B$. The internal redistribution of heat due to conduction is governed by the equation

$$\varrho c_p \frac{\partial T}{\partial t} + \frac{\partial Q^c}{\partial z} = 0 \quad (78)$$

Vertical integration gives

$$\varrho c_p h \frac{d\bar{T}}{dt} + Q_S^c - Q_B^c = 0 \quad (79)$$

On combining with (77) we get

$$(Q + Q_S^c) - (Q_B^c - Q^o) = -\varrho L \left(\frac{dz_S}{dt} - \frac{dz_B}{dt} \right) \quad (80)$$

It is easy to separate latent heat budgets at surface and bottom, respectively. At the surface we get

$$Q + Q_S^c = -\rho L \frac{dz_S}{dt} \quad (81)$$

while at the bottom

$$-Q_B^c + Q^o = \rho L \frac{dz_B}{dt} \quad (82)$$

Both balances follow one and the same pattern: The inequality (jump) of heat fluxes at the interfaces (ice-atmosphere, ice-ocean) gives rise to either growing or melting.

However, there is an important distinction, and we have to differentiate between surface and bottom.

At bottom, the ice temperature remains fixed. It is always held at melting temperature, irrespective of any growth or melting. Dependent on lack or surplus of heat flux into the interface, there is loss or gain of latent heat at the interface, i.e. growth or melting.

At surface, the temperature is free to attain any value not greater than melting temperature. It is unknown a priori. Conversion of latent heat is possible for melting only - growth by freezing of water being excluded -, but melting occurs only after heating up the ice to the melting temperature. Thus, there are unilateral constraints to both surface temperature and conversion of latent heat. Yet, we only have either heating/cooling or melting. These two distinct regimes are associated with the following two disjoint cases:

1. As long as $T_{surf} \leq T_{melt}$ or $Q + Q_S^c \leq 0$, equation (82) should be regarded as a condition on the surface temperature which as well is found from $Q + Q_S^c = 0$. Any change in the control is matched by adjustment of the surface temperature.

2. If both $T_{surf} = T_{melt}$ and $Q + Q_S^c > 0$, the melting temperature has already been reached as an insurmountable obstacle, yet even more heat is supplied to the surface. In this case, there is no reasonable surface temperature $T_{surf} \leq T_{melt}$ that satisfies the flux balance $Q + Q_S^c = 0$. A defect of heat fluxes comes into play which physically acts a source of latent heat. Equation (82) is recovered. Compliant with the physical meaning of the melting term, we always have $\frac{dz_s}{dt} \leq 0$. If it is impossible to satisfy $Q + Q_S^c = 0$ with then melting is required to hold the balance. (Incidentally, the budget then reduces to $Q = -\rho L \frac{dz_s}{dt}$.) Hence, in the case $T_{surf} = T_{melt}$ and $Q + Q_S^c > 0$, equation (81) gives the rate of surface melting.

We prefer to tackle (81) in the form

$$Q + Q_B^c = \rho c_p h \frac{d\bar{T}}{dt} - \rho L \frac{dz_S}{dt} \quad (83)$$

where use was made of (79). On adding (82) and (83), we again arrive at the commencing heat budget equation (77).

To close the system at this point, we refer back to some relationship between mean (bulk) temperature and surface temperature, as comes from a hypothesized temperature profile within the ice slab.

As explained, use is made of eqn. (83) to control both ice temperature changes and surface melting. Thus, equation (83) governs both \bar{T} and z_S . But, at any time, only one of these quantities is actually affected.

In standard papers, (83) is found without the heat storage term. But we have found that it is convenient to include as it helps damp rapid fluctuations of the ice temperature which otherwise are common-place. In a quasi-static balance the ice temperature sensitively responds to changes of the atmospheric conditions. By incorporating the full heat budget, the ice temperature is made more physical, perhaps worth comparing with remote pictures, if available.

Once individual ice formation rates are calculated at surface and bottom, the total change of ice thickness finally is $\frac{dh}{dt} = \frac{dz_S}{dt} - \frac{dz_B}{dt}$.

On leads (fractions of open water) there is also ice formation. As long as there is any ice around, the sea surface temperature is held at the melting temperature, and the latent heat budget is governed by

$$Q + Q^o = -\rho L \frac{dh}{dt}, \quad (84)$$

the same principle as for ice formation at the bottom of the ice sheet.

At this point, it should be noted that there are three modes for computing the atmospheric heat flux Q : 1. over open ocean without ice cover 2. over open water /leads) within ice cover 3. over ice sheets. Each regime is associated with its special regime of the surface temperatures which also differ according to the listed three states of surface.

The total ammount of ice formation on the ice fraction and the open water water fraction is the weighted sum of both.

$$\frac{dh}{dt}|_{tot} = A \frac{dh}{dt}|_{slab} + (1 - A) \frac{dh}{dt}|_{lead} \quad (85)$$

In calculating $\frac{dh}{dt}|_{slab}$ the slab thickness is assumed to be h/A as if all the ice were piled up on the covered fraction.

Following Hibler, the thermodynamic evolution of compactness is given by

$$\frac{dA}{dt} = \frac{A}{2h} \min\left(\frac{dh}{dt}|_{tot}, 0\right) + \frac{1 - A}{h_0} \max\left(\frac{dh}{dt}|_{lead}, 0\right) \quad (86)$$

5 Numerical solution technique

5.1 Space discretization

A number of options exists for the choice of the horizontal and vertical arrangement of variables. The most widely used in ocean modelling is the so called C-grid [Arakawa and Lamb 1977], see figure 5. The advantage of this grid lies in better dispersion properties and improvements in the geostrophic adjustment process as long as the horizontal resolution is less than the scale of the Rossby radius. For the baroclinic part, the Rossby radius is typically of the order of 4 – 8 km in the Baltic Sea compared to the present resolution of the model, which is approximately 1.8 km. In the vertical, a z-coordinate system is used with fixed levels in a non-uniform distribution and the thickness of the bottom layer depends on the local depth. The variables are arranged so that vertical velocity is defined at the top and bottom of a grid cell while density is defined in the middle of the cell, see figure 6. As a general rule of space discretization we use central difference approximation of derivatives and averages wherever required.

5.2 Time discretization

A two-level time-stepping is the general scheme. Horizontal advection of momentum, salinity and temperature as well as ice and the horizontal turbulent fluxes are treated explicitly. A shock capturing advection scheme is used for salinity and temperature. Implicit components are barotropic gravity terms in the momentum and continuity equations and vertical exchange of momentum, salinity and temperature. An iterative procedure with a sequence of linearizations is used for ice dynamics, interaction of momentum balance and constitutive equations. The sea ice part consists of a system of highly nonlinear equations comprising the entire ice cover.

In principle, the computational flow chart can shortly be described as follows:

- Thermodynamics of ice - nonlinear equations - cell by cell.
- Blocks of numerical treatment within time loop:
 1. horizontal stress, eddy viscosity with respect to the vertical.
 2. calculation of density, hydrostatic equation.
 3. equation of continuity, momentum equations.
 4. advection and diffusion of salinity and temperature.
 5. dynamics of ice, ice momentum balance and constitutive equations.
 6. advection of ice (thickness, compactness, snow cover).
 7. heat flow at surface, thermodynamics of sea ice.
 8. effects of surface waves.

9. one-way control of dynamics to nested grids.
10. two-way exchange of salinity and temperature at grid joints.

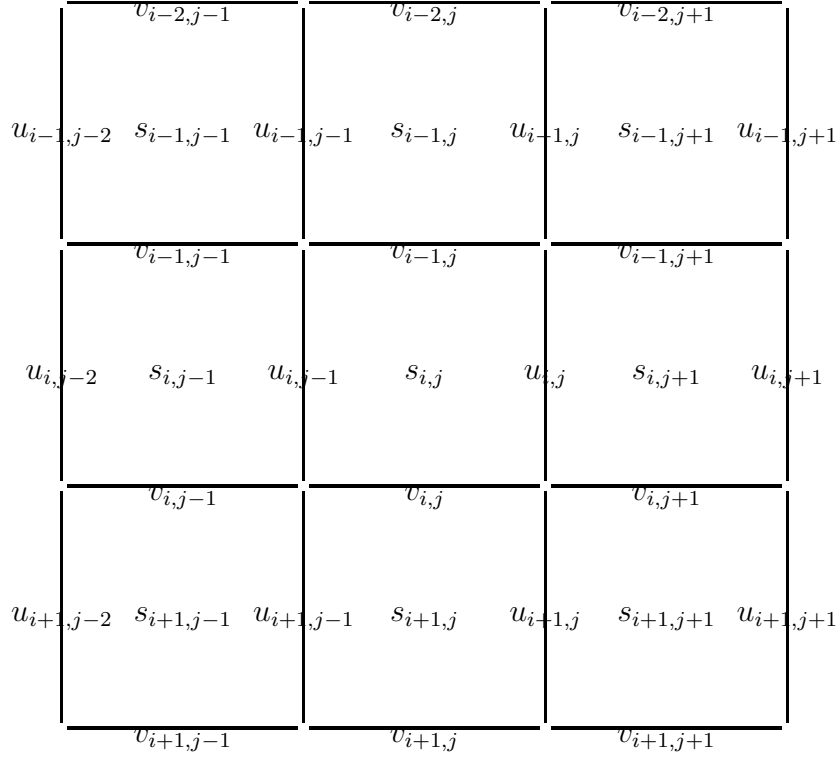


Figure 5: Horizontal distribution of variables on a C-grid. s , u and v stand for salinity, u -velocity and v -velocity component resp. Note that the origo is located at the upper left corner of the grid and the indices are arranged in accordance with conventional matrix indexing

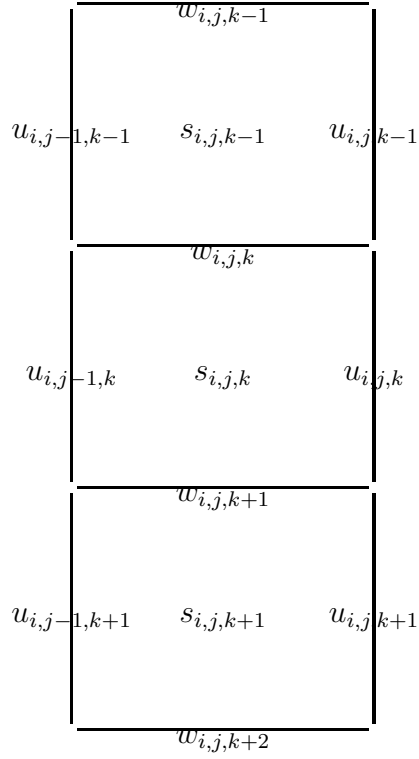


Figure 6: Vertical distribution of variables where s , u and w stand for salinity, u-velocity and w-velocity component resp.

6 Parallelization

Before the breakthrough of modern supercomputers with distributed memory and a large number of processors working in parallel, ocean model codes were often written in Fortran 77. However, to really utilise the efficiency of both shared memory vector computers and distributed memory parallel computers, it has been necessary to at least rewrite some of the code in Fortran 90.

Unlike atmospheric models, where all the grid points in the model are active, ocean models contain a large number of land points. The computational domain therefore has to be partitioned into blocks containing a minimum of inactive points.

Accordingly, the task of parallelization the original HIROMB code has been divided into two main parts; rewriting of the code to take advantage of the Fortran 90 features and dividing the model area into blocks with a minimum of inactive points. A further part is the exchange of numerical algorithms especially designed for distributed memory parallel computers.

For more details concerning the parallelization, the reader is referred to the work by Tomas Wilhelmsson, Josef Schüele and Jarmo Rantakokko, [Wilhelmsson and Schüele 1998] and [Rantakokko 1997].

6.1 Modification of the code

To minimize the coding work, most of the original Fortran 77 code has been kept intact except where new numerics has been added. The modification of the code has mainly consisted of using pointers to switch between the blocks and different grids. The Message Passing Interface (MPI) library has been used for communication between processors.

One of the most time-consuming parts in the code comes from the implicit solver that is used for both the barotropic part and the ice module. Therefore the old serial solver has been exchanged with a new distributed multi-frontal solver written by Bruce Herndon [Herndon 1996]. New software for parallel architectures are becoming available and in the test runs we also have done experiments with the multi-frontal solver MUMPS [Amestoy et al. 1998]. However, for our special application, the performance of the Herndon's solver has shown to be superior.

6.2 Decomposition into blocks

In the computational domain that covers the whole 1 nm grid, only 26% of the surface points and less than 10% of the volume points are active points. Thus the main task of the decomposition is to cut off as much as possible of the non-active grid points. This is achieved by decomposing the domain into blocks that contain as less as possible of the land points. At the same time, there has to be a limit on the number of blocks, because the more blocks the more work is spent on overhead from switching block context and updating block boundaries. A careful examination of how the performance rate depends on the distribution and number of blocks is therefore necessary to arrive at the optimum block decomposition. Because of the implicit treatment of the vertical diffusion it is an advantage if the decomposition is done only in the horizontal. Then a further reduction is possible by eliminating non-active deeper layers.

To carry out this procedure, we have used a newly revised version of the domain decomposition package of Jarmo Rantakokko [Rantakokko 1997]. Measure-

ments described in [Wilhelmsson and Schüle 1998] shows that an inactive land point uses almost 40% of the time of an active water point. An outline of the decomposition algorithm is described below.

1. The domain is first split into halves and the two resulting blocks are shrunk to remove inactive points.
2. The first step is repeated a number of times, where blocks with a lower than average fraction of active points are split and then shrunk. In this manner the fraction of active points is kept up in the blocks.
3. The blocks are distributed onto the processors with the recursive spectral bisection (RSB) method. If the resulting load imbalance is above a given threshold, blocks are split further until the load imbalance is below the threshold.
4. Where possible, blocks on the same processor are combined and merged together in order to reduce the number of communication points within each processor.
5. As a final step, the number of inactive points is reduced further by shrinking the blocks where possible.

6.2.1 Decomposition of ice coverage

Even with the introduction of the new distributed solver for the implicit solution of the ice equations, the ice module still accounts for a large part of the total execution time as soon as the ice coverage reaches normal values. The dynamic nature of the ice coverage requires a time-dependent decomposition which is different from the one for the water part. Special care also has to be taken to areas where ice will form as the computation of the forecast proceeds. To manage this, the area occupied with ice has been extended to include areas with a sea surface temperature below a given value. Figure 7 shows an example of two decompositions of the same 1 nm grid, one for water and one for ice. Experiments with equal and different number of blocks for the water and ice part have shown that the best performance is achieved by using less blocks for the ice part compared to the water part.

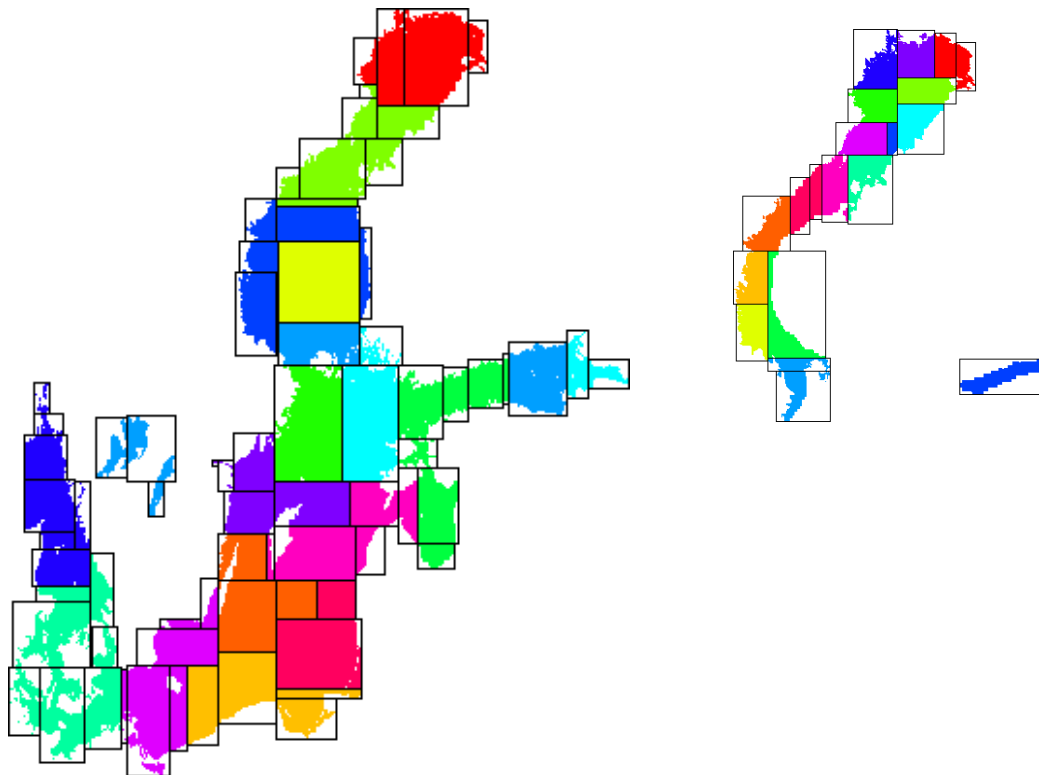


Figure 7: Two decompositions of the 1 nm grid for water on the left and for ice on the right. The initial ice decomposition consists of 20 blocks on 16 processors. (From [Wilhelmsson and Schüle 1998])

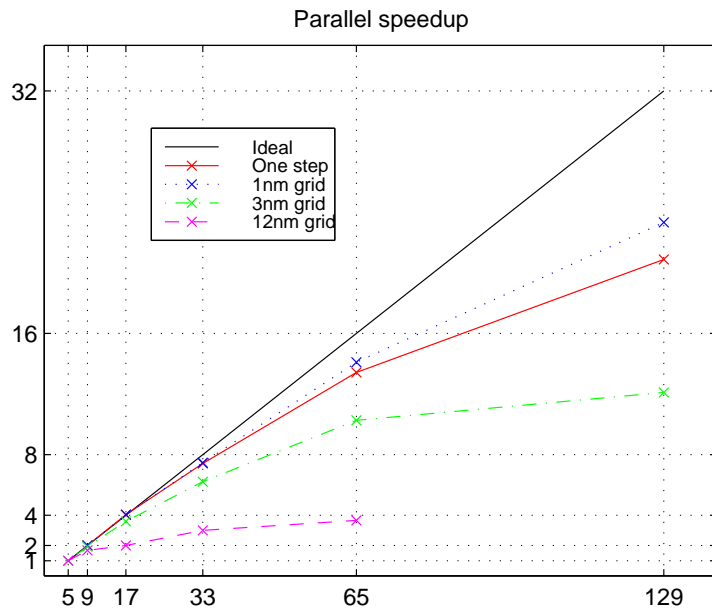


Figure 8: Speedup as a function of the number of PE's as given in Table 2. Note that the baseline for the 12 *nm* and 3 *nm* grids is 1.0 with 5 PE's. For the 1 *nm* grid and the whole time step, the baseline is 2.0 with 9 PE's. (From [Wilhelmsson and Schüle 1998])

#PE	12 nm grid		3 nm grid		1 nm grid		Whole time step	
	Time	Speedup	Time	Speedup	Time	Speedup	Time	Speedup
5	0.67	1.0	5.75	1.0	Out of memory		Out of memory	
9	0.40	1.7	2.98	1.9	28.97	1.0	32.98	1.0
17	0.34	2.0	1.60	3.6	14.34	2.0	16.31	2.0
33	0.22	3.0	0.92	6.2	7.75	3.7	8.87	3.7
65	0.18	3.7	0.56	10.3	4.11	7.0	4.90	6.7
129	0.17	3.9	0.47	12.1	2.48	11.7	3.15	10.4

Table 2: Timings for one whole time step using a dataset without ice from July 1, 1999. Herndon’s solver was used in all timings, except for the 1 nm grid and whole step execution on the 9 PEs, which used the MUMPS solver due to memory constraints. In the 129 PE timing, the 12 nm grid was only distributed onto 64 PEs. (From [Wilhelmsson and Schüle 1998])

6.2.2 Data handling

A master processor takes care of the assembling, packing, and writing data and is to some extent overlapping computations done by the working processors. This is a very important point in achieving parallel efficiency. The Herndon’s solver [Herndon 1996] requires the working processors to be a power of two, implying that with the master processor included, $2^n + 1$ processors are used in the simulations. The master processor is also responsible for updating and distributing external boundaries to the working processors.

6.2.3 Parallel performance

Table 2 (from [Wilhelmsson and Schüle 1998]) illustrates the performance obtained so far on a CRAY T3E-600, and figure 8 (from [Wilhelmsson and Schüle 1998]) illustrates the parallel speedup for one full time step without ice. A 48-hour forecast with the 1 nm grid included needs approximately 30 minutes CPU-time on 65 PE’s on a T3E with the ice excluded.

Acknowledgement This work has been financed by Bundesamt für Seeschifffahrt und Hydrographie (BSH), Hamburg and the Swedish Meteorological and Hydrological Institute.

References

- [Amestoy et al. 1998] P.R. Amestoy, I.S. Duff and J-Y. L’Excellent (1998). *MUMPS multifrontal massively parallel solver version 2.0*. Technical Report TR/PA/98/02, CERFACS.

- [Arakawa and Lamb 1977] A. Arakawa and V.R. Lamb (1977). *A potential enstrophy and energy conserving scheme for the shallow water equation* Mon. Wea. Rev., **109**, 18-36.
- [Blumberg and Mellor 1987] A. F. Blumberg and G. L. Mellor (1987). *A description of a three-dimensional coastal ocean circulation model* Three-Dimensional Coastal ocean Models, edited by N. Heaps, 208 pp., American Geophysical Union, 1987.
- [Boussinesq 1877] M. J. Boussinesq (1877). *Essai sur la theorie des eaux courantes* Memoires presentes par divers savants, A l'academie des sciences de l'institut national de France, tome XXIII, **1**.
- [Elken 1996] J. Elken (1996). *Deep water overflow, circulation and vertical exchange in the Baltic Proper* Report Series, Estonian Marine Institute, Tallinn, No **6**
- [Funkquist and Gidhagen 1984] L. Funkquist and L. Gidhagen (1984). *A model for pollution studies in the Baltic Sea* SMHI Rapporter Hydrologi och Oceanografi **39**. Available from SMHI, S-60176 Norrköping, Sweden.
- [Funkquist 1985] L. Funkquist (1985). *Studies of upwelling in the Baltic Sea with a numerical model* SMHI FoU-Notiser **45**. Available from SMHI, S-60176 Norrköping, Sweden.
- [Funkquist 1993] L. Funkquist (1993). *An operational Baltic Sea circulation model* SMHI Reports Oceanography **18**. Available from SMHI, S-60176 Norrköping, Sweden.
- [Gill 1982] A. E. Gill (1982). *Atmosphere-Ocean Dynamics* International Geophysics Series, **30**, Academic Press.
- [Graham 2000] L. P. Graham (2000). *Large-scale Hydrological Modeling in the Baltic Basin* Ph.D. Thesis, Division of Hydraulic Engineering, Department of Civil and Environmental Engineering, Royal Institute of Technology, 49 pp.
- [Günther and Rosenthal 1983] H. Günther and W. Rosenthal (1983). *Shallow water surface wave model based on the Texel-Marsen-Arsloe (TMA) wave spectrum*. Proceedings of the 20th Congress of the Internat. Association of Hydraulic Research (IAHR), Moscow/SU 1983.
- [Heaps 1974] N. S. Heaps (1974). *Development of a Three-Dimensional Numerical Model of the Irish Sea* Rapp. P.-v. Reun. Cons. int. Explor. Mer. **167**, 147-162.

- [Herndon 1996] B. Herndon (1996). *A Methodology for the Parallelization of PDE solvers: Application to Semiconductor Device Physics* PhD Thesis, Stanford University.
- [Hibler 1979] W. D. Hibler (1979). *A dynamic thermodynamic sea ice model* J.Phys.Oceanogr.**9** (4).
- [HIRLAM 1993] N. Gustafsson, editor (1993). *The HIRLAM 2 Final Report* HIRLAM Technical Report **9**. Available from SMHI, S-60176 Norrköping, Sweden.
- [Idso and Jackson 1969] S.B. Idso and R.D. Jackson (1969). *Thermal radiation from the atmosphere* J.Geophys.Res. **74**, 5397-5403.
- [Karman 1930] Th.von Karman (1930). *Mechanische Ähnlichkeit und Turbulenz* Nachr.d.Ges.d.Wiss.zu Göttingen a. d. Jahre 1930, Math-Phys. Klasse, pp. 58-76.
- [Kielmann 1981] J. Kielmann (1981). *Grundlagen und Anwendung eines numerischen Modells der geschichteten Ostsee* Ber.Inst.f.Merresk., Kiel **87a,b**.
- [Kleine 1993] E. Kleine (1993). *Die Konzeption eines numerischen Verfahrens für die Advektionsgleichung* Bundesamt für Seeschifffahrt und Hydrographie, Hamburg.
- [Kleine 1994] E. Kleine (1994). *Das operationelle Modell des BSH für Nordsee und Ostsee, Konzeption und Übersicht* Bundesamt für Seeschifffahrt und Hydrographie, Hamburg.
- [Kleine and Sklyar 1995] E. Kleine and S Sklyar (1995). *Mathematical feature of Hibler's model of large-scale sea-ice dynamics* Deutsche Hydrographische Zeitschrift, **47(3)**, pp. 179-230.
- [Laikhtman 1979] D.L. Laikhtman (1979). *On the structure of the planetary boundary layer* Phys.Atmos.Oceans (russian) **15**, 983-987.
- [Lehmann 1995] A. Lehmann (1995). *A three-dimensional baroclinic eddy-resolving model of the Baltic Sea* Tellus, **47A**, 1013-1031.
- [Liu et al. 1979] A.J. Liu, K.B. Katsaros and J.A. Businger (1979) *Parametrization of Air-sea Exchange of Heat and Water Vapor Including the Molecular Constraints at the Interface* J.Atmos.Sci **36**, 1722-1735.

- [Mellor and Yamada 1974] G.L. Mellor and T. Yamada (1974). *A hierarchy of turbulence closure models for planetary boundary layers* J.Atmos.Sci **31**, 1791-1806.
- [Omstedt and Rutgersson 1998] A. Omstedt and A. Rutgersson (1998). *Closing the water and heat cycle of the Baltic Sea* Submitted
- [Payne 1972] R.E. Payne (1972). *Albedo of the sea surface* J.Atmos.Sci. **29**, 959-970.
- [Rantakokko 1997] J. Rantakokko (1997). *A framework for partitioning domains with inhomogeneous workload* Technical Report No. **194**, Dep. of Scientific Computing, Uppsala University, Uppsala, Sweden.
- [Reynolds 1895] O. Reynolds (1895). *On the Dynamical Theory of Incompressible Viscous Fluids and the Determination of the Criterion* Philos.Trans.Roy.Soc. London vol.**186**, 123-164.
- [Shine 1984] K.P. Shine (1984). *Parameterization of shortwave flux over high albedo surfaces as function of cloud thickness and surface albedo* Quart.J.Roy.Met.Soc. **110**, 747-761.
- [Simons 1978] T. J. Simons (1978). *Wind-driven circulations in the southwest Baltic* Tellus, **30**
- [Simons et al. 1977] T. J. Simons, L. Funkquist and J. Svensson (1977). *Application of a numerical model to Lake Vänern* SMHI Rapporter Hydrologi och Oceanografi **9**. Available from SMHI, S-60176 Norrköping, Sweden.
- [Smagorinsky 1963] J. Smagorinsky (1963). *General circulation experiments with primitive equations, I. The basic experiment* Mon.Wea.Rev. **91**,99-164
- [Stokes 1845] G.G. Stokes (1845). *On the Theories of the Internal Friction* Quart.J.Roy.Met.Soc. **110**, 747-761.
- [Vasseur et al. 1980] B. Vasseur, L. Funkquist and J. F. Paul (1980). *Verification of a numerical model for thermal plumes* SMHI Rapporter Hydrologi och Oceanografi **24**. Available from SMHI, S-60176 Norrköping, Sweden.
- [Wilhelmsson and Schüle 1998] T. Wilhelmsson and J. Schüle (1998). *Parallelizing the Operational Ocean Model HIROMB* Technical Report TRITA-NA-**9816**, Department of Numerical Analysis and Computing Science, Royal Institute of Technology, Stockholm, Sweden.

river	mean runoff ($m^3 s^{-1}$)	river	mean runoff ($m^3 s^{-1}$)
Kyroenjoki	44.00	Pregola	87.00
Lapuanjoki	33.00	Neman	674.00
Kalajoki	28.00	Venta	65.00
Pyhäjoki	28.00	Mälaren	156.00
Siikajoki	41.00	Nyköpingsån	21.00
Oulujoki	260.00	Motala ström	96.00
Iijoki + Kiiminkijoki	220.00	Emån	28.00
Simojoki	38.00	Mörrumsån	27.00
Kemijoki	578.00	Helge å	48.00
Torne älv	388.00	Rönne å	21.00
Kalix älv	290.00	Lagan	71.00
Råne älv	44.00	Nissan	40.00
Lule älv	508.00	Ätran	46.00
Pite älv	170.00	Viskan	30.00
Skellefte älv	160.00	Randers fjord	100.00
Kokemäenjoki	221.00	Göta älv	530.00
Ume älv	423.00	Glomma	600.00
Öre älv	35.00	Oslofjord	300.00
Gide älv	35.00	Lågen	600.00
Ångermanälven	480.00	Nidelv	245.00
Indalsälven	439.00	Otra/Tovdalselv	400.00
Ljungan	140.00	Firth of Forth	555.00
Ljusnan	230.00	Humber/Tyne	290.00
Dalälven	370.00	Thames	100.00
Narva	357.00	Seine	400.00
Luga	90.00	Scheldt	150.00
Neva	2600.00	Rhein/Meuse	2380.00
Kymijoki	368.00	N Sea channel	90.00
Kasari	24.00	IJsselmeer, Waddenzee	500.00
Pärnu	48.00	Ems/Dollart	100.00
Salatsa	30.00	Weser	450.00
Gauya	68.00	Elbe	900.00
Daugava + Lielupe	723.00	Ringkøbing fjord	125.00
Oder	522.00	Kvina/Sira	300.00
Rega	21.00	Lysefjord	100.00
Parseta	28.00	Boknafjord	485.00
Vistula	1010.00		

Table 3: Annual mean of river runoff

8 SMHI Publications

SMHI publish seven reportseries. Three of these, the R-series, are intended for international readers and are in most cases written in English. For the others the Swedish language is used.

Name of the series	Published since
RMK (Report Meteorology and Climatology)	1974
RH (Report Hydrology)	1990
RO (Report Oceanography)	1986
METEOROLOGI	1985
HYDROLOGI	1985
OCEANOGRAFI	1985
KLIMATOLOGI	2009

Earlier issues published in RO

1	Lars Gidhagen, Lennart Funkquist and Ray Murthy (1986) Calculations of horizontal exchange coefficients using Eulerian time series current meter data from the Baltic Sea.	Program för miljö kvalitetsövervakning - PMK. Utsjöprogram under 1987
2	Thomas Thompson (1986) Ymer-80, satellites, arctic sea ice and weather.	8 Bertil Håkansson (1988) Ice reconnaissance and forecasts in Storfjorden, Svalbard.
3	Stig Carlberg et al (1986) Program för miljö kvalitetsövervakning - PMK.	9 Stig Carlberg, Sven Engström, Stig Fonselius, Håkan Palmén, Eva-Gun Thelén, Lotta Fyrberg, Bengt Yhlen, Danuta Zagradkin, Bo Juhlin och Jan Szaron (1989) Program för miljö kvalitetsövervakning - PMK. Utsjöprogram under 1988.
4	Jan-Erik Lundqvist och Anders Omstedt (1987) Isförhållandena i Sveriges södra och västra farvatten.	10 L. Fransson, B. Håkansson, A. Omstedt och L. Stehn (1989) Sea ice properties studied from the ice-breaker Tor during BEPERS-88.
5	Stig Carlberg, Sven Engström, Stig Fonselius, Håkan Palmén, Eva-Gun Thelén, Lotta Fyrberg och Bengt Yhlen (1987) Program för miljö kvalitetsövervakning - PMK. Utsjöprogram under 1986.	11 Stig Carlberg, Sven Engström, Stig Fonselius, Håkan Palmén, Lotta Fyrberg, Bengt Yhlen, Bo Juhlin och Jan Szaron (1990) Program för miljö kvalitetsövervakning - PMK. Utsjöprogram under 1989.
6	Jorge C. Valderama (1987) Results of a five year survey of the distribution of UREA in the Baltic sea.	12 Anders Omstedt (1990) Real-time modelling and forecasting of temperatures in the Baltic Sea.
7	Stig Carlberg, Sven Engström, Stig Fonselius, Håkan Palmén, Eva-Gun Thelén, Lotta Fyrberg, Bengt Yhlen och Danuta Zagradkin (1988).	13 Lars Andersson, Stig Carlberg, Elisabet Fogelqvist, Stig Fonselius, Håkan Palmén, Eva-Gun Thelén, Lotta Fyrberg, Bengt Yhlen och Danuta Zagradkin (1991)

- Program för miljökvalitetsövervakning – PMK. Utsjöprogram under 1989.
- Application of the BSH model to Kattegat and Skagerrak.
- 14 Lars Andersson, Stig Carlberg, Lars Edler, Elisabet Fogelqvist, Stig Fonselius, Lotta Fyrberg, Marie Larsson, Håkan Palmén, Björn Sjöberg, Danuta Zagradkin, och Bengt Yhlen (1992)
Haven runt Sverige 1991. Rapport från SMHI, Oceanografiska Laboratoriet, inklusive PMK - utsjöprogrammet. (The conditions of the seas around Sweden. Report from the activities in 1991, including PMK - The National Swedish Programme for Monitoring of Environmental Quality Open Sea Programme.)
 - 15 Ray Murthy, Bertil Håkansson and Pekka Alenius (ed.) (1993)
The Gulf of Bothnia Year-1991 - Physical transport experiments.
 - 16 Lars Andersson, Lars Edler and Björn Sjöberg (1993)
The conditions of the seas around Sweden. Report from activities in 1992.
 - 17 Anders Omstedt, Leif Nyberg and Matti Leppäranta (1994)
A coupled ice-ocean model supporting winter navigation in the Baltic Sea. Part 1. Ice dynamics and water levels.
 - 18 Lennart Funkquist (1993)
An operational Baltic Sea circulation model. Part 1. Barotropic version.
 - 19 Eleonor Marmefelt (1994)
Currents in the Gulf of Bothnia. During the Field Year of 1991.
 - 20 Lars Andersson, Björn Sjöberg and Mikael Krysell (1994)
The conditions of the seas around Sweden. Report from the activities in 1993.
 - 21 Anders Omstedt and Leif Nyberg (1995)
A coupled ice-ocean model supporting winter navigation in the Baltic Sea. Part 2. Thermodynamics and meteorological coupling.
 - 22 Lennart Funkquist and Eckhard Kleine (1995)
 - 23 Tarmo Kõuts and Bertil Håkansson (1995)
Observations of water exchange, currents, sea levels and nutrients in the Gulf of Riga.
 - 24 Urban Svensson (1998)
PROBE An Instruction Manual.
 - 25 Maria Lundin (1999)
Time Series Analysis of SAR Sea Ice Backscatter Variability and its Dependence on Weather Conditions.
 - 26 Markus Meier¹, Ralf Döscher¹, Andrew, C. Coward², Jonas Nycander³ and Kristofer Döös³ (1999). RCO – Rossby Centre regional Ocean climate model: model description (version 1.0) and first results from the hindcast period 1992/93.
- ¹ Rossby Centre, SMHI ² James Rennell Division, Southampton Oceanography Centre, ³ Department of Meteorology, Stockholm University
- 27 H. E. Markus Meier (1999)
First results of multi-year simulations using a 3D Baltic Sea model.
 - 28 H. E. Markus Meier (2000)
The use of the $k - \epsilon$ turbulence model within the Rossby Centre regional ocean climate model: parameterization development and results.
 - 29 Eleonor Marmefelt, Bertil Håkansson, Anders Christian Erichsen and Ian Sehested Hansen (2000)
Development of an Ecological Model System for the Kattegat and the Southern Baltic. Final Report to the Nordic Councils of Ministers.
 - 30 H.E Markus Meier and Frank Kauker (2002).
Simulating Baltic Sea climate for the period 1902-1998 with the Rossby Centre coupled ice-ocean model.
 - 31 Bertil Håkansson (2003)
Swedish National Report on Eutrophication Status in the Kattegat and

the Skagerrak OSPAR ASSESSMENT
2002

operational baroclinic model for the Baltic
Sea

- 32 Bengt Karlson & Lars Andersson (2003)
The Chattonella-bloom in year 2001 and
effects of high freshwater input from river
Göta Älv to the Kattegat-Skagerrak area
- 33 Philip Axe and Helma Lindow (2005)
Hydrographic Conditions Around Offshore
Banks
- 34 Pia M Andersson, Lars S Andersson
(2006)
Long term trends in the seas surrounding
Sweden. Part one - Nutrients
- 35 Bengt Karlson, Ann-Sofi Rehnstam-Holm
& Lars-Ove Loo (2007)
Temporal and spatial distribution of
diarrhetic shellfish toxins in blue mussels,
Mytilus edulis (L.), at the Swedish West
Coast, NE Atlantic, years 1988-2005
- 36 Bertil Håkansson
Co-authors: Odd Lindahl, Rutger
Rosenberg, Philip Axe, Kari Eilola, Bengt
Karlson (2007)
Swedish National Report on
Eutrophication Status in the Kattegat and
the Skagerrak OSPAR ASSESSMENT
2007
- 37 Lennart Funkquist and Eckhard Kleine
(2007)
An introduction to HIROMB, an
- 38 Philip Axe (2008)
Temporal and spatial monitoring of
eutrophication variables in CEMP
- 39 Bengt Karlson, Philip Axe, Lennart
Funkquist, Seppo Kaitala, Kai Sørensen
(2009)
Infrastructure for marine monitoring and
operational oceanography
- 40 Marie Johansen, Pia Andersson (2010)
Long term trends in the seas surrounding
Sweden
Part two – Pelagic biology
- 41 Philip Axe, (2010)
Oceanographic Applications of Coastal
Radar
- 42 Martin Hansson, Lars Andersson, Philip
Axe (2010)
Areal Extent and Volume of Anoxia and
Hypoxia in the Baltic Sea, 1960-2010



Swedish Meteorological and Hydrological Institute
SE 601 76 NORRKÖPING
Phone +46 11-495 80 00 Telefax +46 11-495 80 01

ISSN 0283-1112